Available online at www.sciencedirect.com
ScienceDirect
Journal of the European Ceramic Society 30 (2010) 1955–1962
www.elsevier.com/locate/jeurceramsoc

A new route to fabricate SiB_4 modified C/SiC composites

Fengming Shi, Xiaowei Yin*, Xiaomeng Fan, Laifei Cheng, Litong Zhang

National Key Laboratory of Thermostructure Composite Materials, Northwestern Polytechnical University, West Youyi Rd., No. 127, Xi'an, Shaanxi 710072, PR China

Received 21 December 2009; received in revised form 10 February 2010; accepted 27 February 2010
Available online 26 March 2010

Abstract

In order to improve the oxidation and thermal shock resistance of 2D C/SiC composites, dense SiB_4–SiC matrix was in situ formed in 2D C/SiC composites by a joint process of slurry infiltration and liquid silicon infiltration. The synthesis mechanism of SiB_4 was investigated by analyzing the reaction products of B_4C–Si system. Compared with the porous C/SiC composites, the density of C/SiC–SiB_4 composites increased from 1.63 to 2.23 g/cm^3 and the flexural strength increased from 135 to 330 MPa. The thermal shock behaviors of C/SiC and C/SiC–SiB_4 composites protected with SiC coating were studied using the method of air quenching. C/SiC–SiB_4 composites displayed good resistance to thermal shock, and retained 95% of the original strength after being quenched in air from 1300 °C to room temperature for 60 cycles, which showed less weight loss than C/SiC composite.

Keywords: Composites; Fibers; Thermal shock resistance; Borides; Carbides

1. Introduction

Continuous carbon fiber reinforced silicon carbide matrix composites (C/SiC) exhibit attractive properties for high temperature structural applications because of their low density, high strength, non-brittle mechanical behavior, good fatigue resistance and good oxidation resistance at high temperatures.[1–5] However, C/SiC composites fabricated by chemical vapor infiltration (CVI) have large residual pores located among fiber bundles and matrix/coating micro-cracks resulted from the coefficient of thermal expansion (CTE) mismatch.[6–8] Oxidizing species can diffuse through these pores and micro-cracks, leading to the oxidation of pyrolytic carbon (PyC) interphase and carbon fibers at high temperatures.[9,10] Therefore, for long-term use at elevated temperatures, various efforts have being expended on attempting to improve the oxidation resistance of C/SiC composites.

Boron-bearing species are effective to improve the oxidation resistance of C/SiC composites at relatively low temperatures (500–1000 °C). They can form liquid oxide phase (B_2O_3 or B–M–O ternary phase) during oxidation to fill cracks, slowing down the in-depth diffusion of oxygen.[1,11] In our previous work, SiO_2–B_2O_3 glass was introduced into C/SiC composites. As a good sealant, SiO_2–B_2O_3 glass filled the existing crack network at the temperatures ranging from 500 to 1100 °C and effectively improved the oxidation resistance of the composites.[10] However, SiO_2–B_2O_3 glass itself has low softening temperature which may limit the application of C/SiC composites at elevated temperatures. Therefore, a kind of matrix which has high melting point and low liquid formation temperature is needed. Silicon tetraboride (SiB_4) has a melting point of 1920 °C and its liquid formation temperature is low.[12] In the previous work, SiB_4 particles as self-healing filler were infiltrated into the inter-bundle pores of 2D C/SiC composites by slurry infiltration (SI) combined with CVI SiC to improve the oxidation resistance of composites. The oxidation of SiB_4 can lead to the formation of fluid oxide phase SiO_2–B_2O_3, which can hinder the inwards diffusion of oxygen and protect the PyC interphase and carbon fibers from being oxidized.[13,14] However, the SiB_4–SiC matrix was not dense because of the bottleneck effect of CVI, which restricted its oxidation resistance at high temperatures.

In a word, it is necessary to form dense and homogeneous self-healing SiB_4 matrix in porous 2D C/SiC composites. SI has been proved to be a viable approach to introduce ceramic particles into fiber reinforced ceramic matrix composites.[14–16] Liquid silicon infiltration (LSI) is an effective method to fabricate high-density,

* Corresponding author. Tel.: +86 29 88494947; fax: +86 29 88494620.
E-mail address: yinxw@nwpu.edu.cn (X. Yin).

0955-2219/$ – see front matter © 2010 Elsevier Ltd. All rights reserved.
doi:10.1016/j.jeurceramsoc.2010.02.028

near net-shaped C/SiC composites at significantly reduced cost. During LSI, liquid silicon is sucked into the preform by capillary force at temperatures well above the melting point of silicon in vacuum.[17–20] The wettability of liquid silicon in the porous preform determines the extent and rate of spontaneous infiltration. Under vacuum, liquid silicon has favorable wettability on boron carbide (B_4C) at temperatures above 1410 °C.[21] Therefore, a joint process of SI and LSI can be a good solution of introducing B_4C particles and molten silicon into the porous C/SiC composite, leading to the in situ formation of SiB_4 by controlling the content of B_4C particles and the reaction temperature. Besides the short period of SI, infiltration time of LSI is much shorter (in minutes). Therefore, the above joint process can dramatically shorten the fabrication period of SiB_4 modified C/SiC composites, which is cost-effective.

In the present work, the synthesis mechanism of SiB_4 by the reaction between B_4C particles and liquid silicon was studied. The microstructures, mechanical properties as well as thermal shock resistance of SiB_4 modified C/SiC composites were investigated in comparison with those of C/SiC composites prepared by CVI.

2. Experimental

Carbon fiber preforms were prepared by stacking plain weave carbon cloths (1 K, T-300, Toray Co., Japan) in a perforated graphite holder, which was tightened to obtain the desired fiber volume fraction (40 vol.%). PyC interphase with a thickness of 0.2 μm was deposited on the fiber using C_3H_6 precursor at 850 °C for 144 h at a reduced pressure of 5 kPa and then heat-treated in argon atmosphere at 1800 °C for 1 h. The as-treated carbon fiber preforms were employed to fabricate a porous 2D C/SiC composite by low-pressure chemical vapor infiltration (LPCVI).[22] These porous C/SiC composites were machined and polished into samples with a dimension of 3.0 mm × 5.0 mm × 40.0 mm which were denoted as sample A. Sample A were infiltrated with B_4C slurry, dried in a vacuum freeze drier, and the as-received materials were denoted as sample C. The slurry was prepared by dispersing B_4C powders (D_{50} = 1.5 μm, 50 wt.%) in deionized water and ball milled for 24 h. Sample C were infiltrated with molten silicon at 1500 °C under vacuum for 5 min, and the as-received materials were denoted as sample D. Two layers of CVD SiC coating were deposited on sample D, and the as-received materials were denoted as sample E. As a comparison, two layers of CVD SiC coating were also deposited on sample A, the as-received materials were denoted as sample B. The schematic of the fabrication procedure of samples is presented in Fig. 1.

In order to reveal the synthesis mechanism of SiB_4, the reaction products of B_4C–Si system were investigated. The raw powders with different molar ratios of B_4C and Si were ball milled. Then the mixed powders were cold-pressed into B_4C/Si compact specimens under the uniaxial pressure of 100 MPa. The B_4C/Si compact specimens were heat-treated in a tube furnace (GSL-1600X, Hefei, China) in argon atmosphere at 1300, 1400 and 1500 °C, respectively.

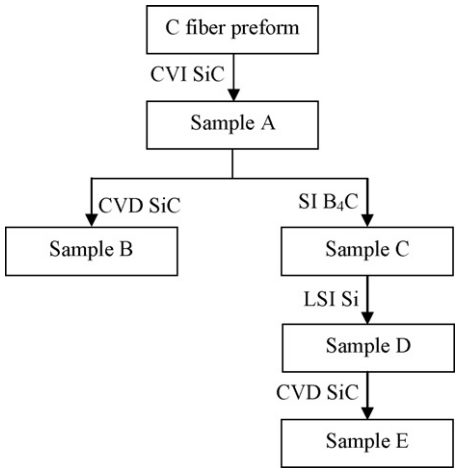

Fig. 1. The schematic of the fabrication procedure of samples.

Thermal shock tests were conducted in static air in a tube furnace. Thermal cycling was carried out between 1300 °C and room temperature in a period of 20 min. Samples B and E were kept in the furnace atmosphere for 10 min and then cooled in air for 10 min. The quenching number was 20, 40 and 60 cycles, respectively. The temperature difference ΔT was 1275 °C. The weight changes of samples were measured by an analytical balance (Mettler Toledo, AG 204, Switzerland) and recorded as a function of quench cycle number. Cumulative weight changes of the samples were calculated using the following equation:

$$\Delta m = \frac{m - m_0}{m_0} \times 100\% \quad (1)$$

where m and m_0 are the weight of the samples after and before thermal shock cycling, respectively. Three to six samples were measured in each case for statistical significance.

Density and open porosity were measured by the Archimedes method with distilled water. The microstructures of the samples were observed under a scanning electron microscopy (SEM, Hitachi, S2700, Japan). The phase composition was measured by X-ray diffraction and microarea X-ray diffraction (XRD, X'pert PRO, Philips, Netherlands) with Cu Kα radiation. The pore size distributions of the samples were measured by Mercury Porosimeter (Poremaster 33, Quantachrome Instruments Corporation, Florida, USA). The flexural strength of the samples was measured via a three-point bending test (SANS CMT 4304, Sans Materials Testing Co., Shenzhen, China) with a span of 30 mm and a loading rate of 0.5 mm/min at room temperature.

3. Results and discussion

3.1. Synthesis mechanism of SiB_4

The atomic structure of B_4C consists of a chain C–B–C and one icosahedron $B_{11}C$ with the carbon atom staying at a polar site.[23] Si atoms may diffuse into the interstitial site of B–C crystal lattice, leading to the formation of solid solution. At elevated temperatures, Si atoms may replace C atoms in the C–B–C chain and icosahedron $B_{11}C$, which leads to the

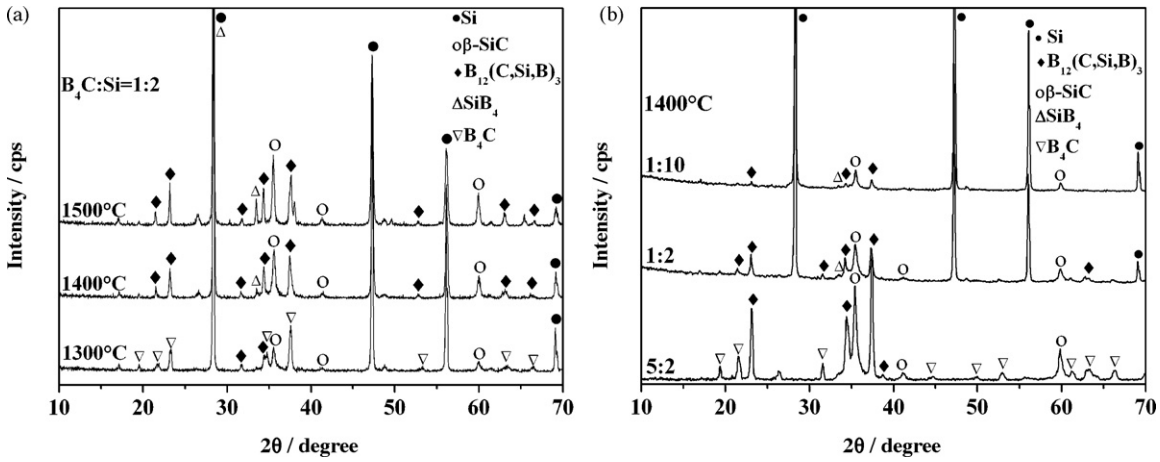

Fig. 2. (a) XRD patterns of B_4C/Si compact specimens with a B_4C/Si molar ratio of 1:2 heat-treated at 1300 °C, 1400 °C and 1500 °C, respectively; (b) XRD patterns of B_4C/Si compact specimens with different B_4C/Si molar ratio heat-treated at 1400 °C.

formation of silicon boride, and the replaced C atoms may react with excess Si, leading to the formation of SiC.

Fig. 2(a) shows the XRD patterns of B_4C/Si compact specimens heat-treated at different temperatures, in which B_4C and Si had a molar ratio of 1:2. According to the XRD pattern of the specimens heat-treated at 1300 °C, main peaks of β-SiC and $B_{12}(C, Si, B)_3$ were identified, besides B_4C and Si in the raw powders. SiC was formed by the reaction between Si and free carbon in the raw powder, and $B_{12}(C, Si, B)_3$ was formed due to the diffusion of Si atoms into the interstitial site of B_4C crystal lattice at 1300 °C. The characteristic peaks of SiB_4 were detected in the specimens heat-treated at 1400 °C. The XRD pattern of the specimens heat-treated at 1500 °C showed an obvious characteristic peak of SiB_4 and the peak intensity was higher than that of 1400 °C, which meant that the content of SiB_4 increased with reaction temperature increasing. To sum up, SiB_4 can form at 1400 °C and the amount increases with the increase of reaction temperature.

Fig. 2(b) shows the XRD patterns of B_4C/Si compact specimens heat-treated at 1400 °C with different molar ratios of B_4C and Si. The XRD pattern of specimen with a B_4C/Si molar ratio of 5:2 showed a part of Si reacted with free carbon to form SiC and others could form $B_{12}(C, Si, B)_3$. With the change of the B_4C/Si molar ratio, the amount of SiB_4 did not change apparently. Known from the above results, the replacement of C atoms in B_4C by Si atoms to form SiB_4 needs higher temperature than the diffusion of Si atoms into the interstitial site of B_4C crystal lattice to form $B_{12}(C, Si, B)_3$.

According to the above results, SiB_4 can be formed by controlling the reaction temperature of B_4C with liquid silicon and their molar ratio. B_4C may be completely transformed into SiB_4 when the temperature is above 1500 °C and the molar ratio between B_4C and Si reaches 1:2.

In the modified C/SiC composites, the molar ratio between B_4C and Si and their reaction temperature can be adjusted during SI and LSI. The reaction is described as:

$$2Si(l) + B_4C(s) \rightarrow SiC(s) + SiB_4(s) \quad (2)$$

During LSI, the vacuum environment can be beneficial to the complete reaction of B_4C with liquid silicon.

3.2. Microstructure and mechanical properties of composites

For CVI C/SiC composites, carbon fibers are protected by PyC interphase and SiC matrix layer. However, there are plenty of pores located among fiber bundles. Fig. 3(a) shows that there are two kinds of pores in sample A, inter-bundle pores and intra-bundle pores, which had a density of 1.63 g/cm^3 and an open porosity of 20% (Table 1).

B_4C slurry was infiltrated into the pores of sample A by a joint process of vacuum infiltration and pressure infiltration until the volume fraction of B_4C reached 8 vol.%. As shown in Fig. 3(b), most of the pores were filled with B_4C particles via SI, and the density of the composite was increased to 1.85 g/cm^3 (Table 1). B_4C filler had little effect on improving the flexural strength of the composites.

LSI procedure involves infiltration and reaction.[24] During LSI procedure, B_4C reacts with liquid silicon, leading to the in situ formation of SiB_4 and SiC phases, SiC crystals grow by the mechanism of recrystallization through the liquid phase.[21] At 1500 °C, reaction between Si and B_4C (molar volume is 22.2 cm^3/mol) with the formation of SiC (molar volume is 12.5 cm^3/mol) and SiB_4 (molar volume is 29.2 cm^3/mol) according to Eq. (2) leads to a volume increase of 87.8%. Thus, the B_4C–Si reaction tends to close the infiltration pore channels in direct competition with the continuing infiltration of liquid silicon into the preform. Therefore, there should be sufficient porosity existing until all B_4C particles are consumed by the reaction.

The infiltration depth of silicon melt among the B_4C particles is determined by the infiltration capillary pressure. Integration of Darcy's law[24]:

$$\frac{dl}{t} = -\frac{K_0 \Delta P}{\eta l} \quad (3)$$

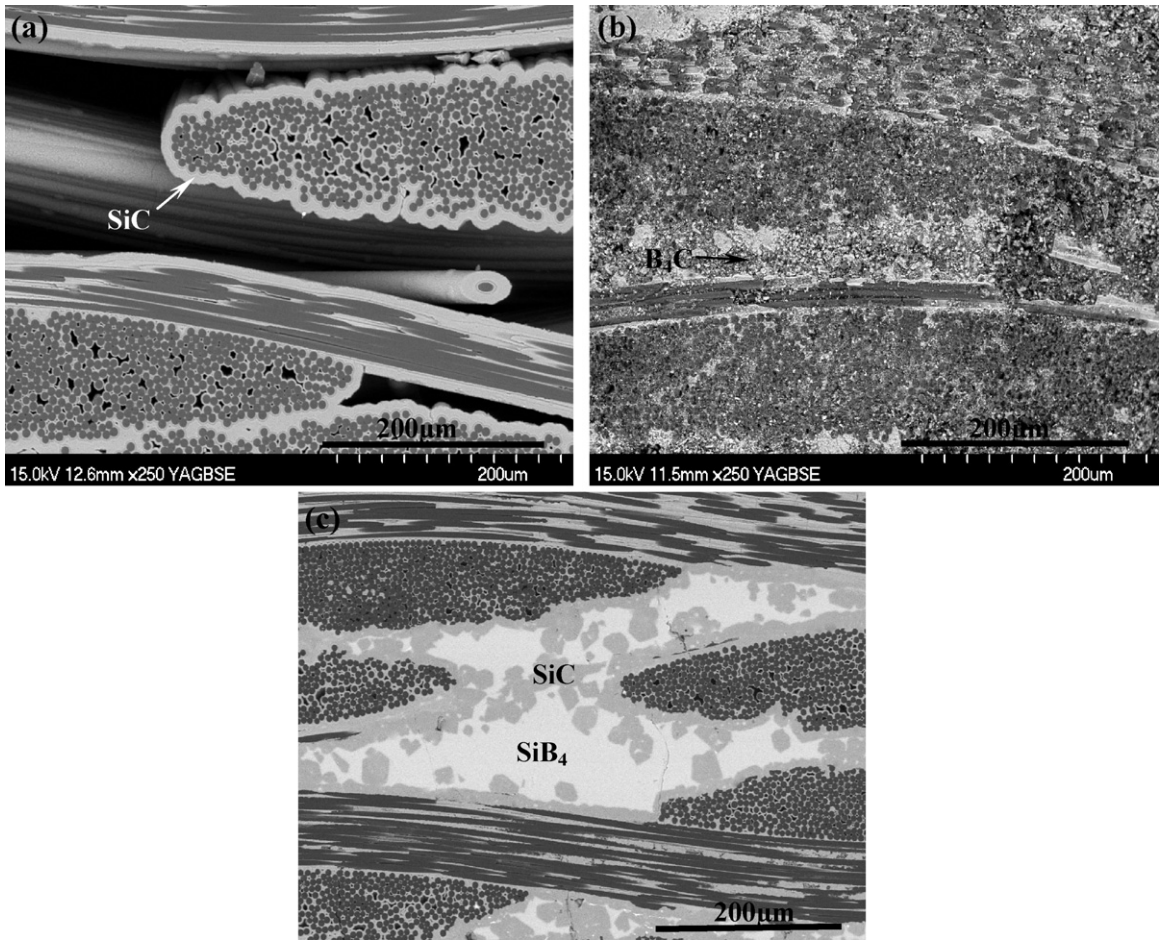

Fig. 3. Back-scattered electron images on the polished cross-section: (a) sample A, showing the inter-bundle pores and the intra-bundle pores; (b) sample C; and (c) sample D.

yields the well-known parabolic law:

$$l^2 = -2\frac{K_0}{\eta}\Delta P t \tag{4}$$

where l is the infiltrated distance, η is the fluid viscosity, K_0 is the constant permeability and t is the infiltration time. ΔP is the infiltration capillary pressure, which can be determined independent of specific pore structures as[25]:

$$\Delta P = \frac{S_P}{V_P}\gamma_{LV}\cos\theta \tag{5}$$

where γ_{LV} is the liquid/vapor interfacial energy, S_P is the pore surface area, V_P is the pore volume and θ is the wetting angle.

According to Eq. (5), at the infiltration temperature, the infiltration capillary pressure increases with the decrease of wetting angle. Under vacuum the wetting angle for liquid silicon on B_4C is as low as 20° at temperatures above 1410 °C,[21] so the infiltrated distance increases quickly with increasing the infiltration time, as known from Eq. (4). Thus, liquid silicon could spontaneously infiltrate into the pores and completely react with B_4C, leading to the formation of SiB_4–SiC binary matrix.

Fig. 4 displays the pore size distributions of samples A, C, and D. Most pores of sample A had a median size of 100 μm, which were located among the fiber bundles. After SI, the inter-bundle pores of sample A were filled with B_4C particles, which divided the pores into smaller ones. Therefore, the average size of the inter-bundle pores in sample C decreased to 10 μm. During LSI, the matrix was further densified by liquid silicon. As a result, there existed only a small quantity of intra-bundle pores in sample D.

Table 1
Properties of various samples.

Samples	Open porosity (%)	Density (g/cm^3)	Flexural strength (MPa)	Flexural modulus (GPa)
Sample A	20	1.63	135 ± 4	25 ± 2
Sample B	9	1.92	222 ± 4	25 ± 2
Sample C	12	1.85	–	–
Sample D	6	2.23	330 ± 19	30 ± 2
Sample E	5	2.36	340 ± 19	36 ± 2

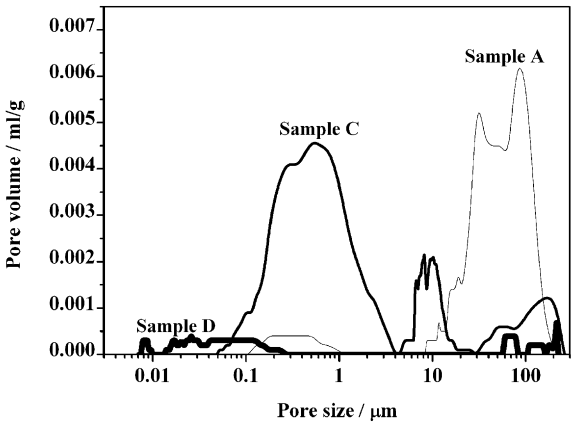

Fig. 4. Pore size distributions of samples A, C and D.

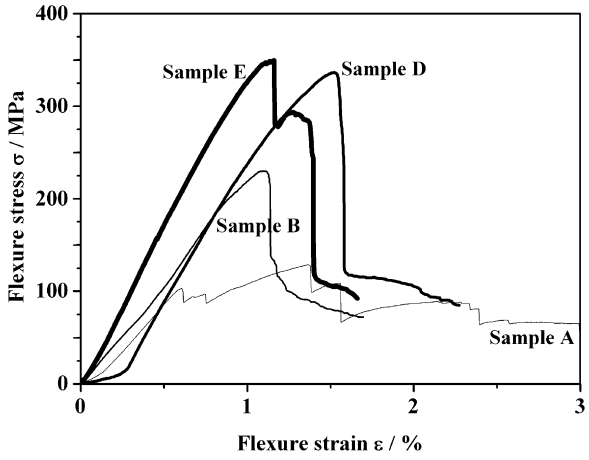

Fig. 6. Flexural stress–strain curves of samples A, B, D and E.

Fig. 5 reveals the phase compositions of four randomly selected microareas in sample D. In these microareas, only carbon, SiC and SiB_4 were found. It illustrated that B_4C has been completely transformed into SiB_4 during LSI under vacuum, in accordance with Eq. (2). Fig. 3(c) shows the polished cross-section of sample D, where dark areas in the original inter-bundle pores represented SiC phase and gray areas SiB_4. It can be seen that the inter-bundle pores of porous composites were filled homogeneously by the in situ formed SiB_4–SiC matrix.

Properties of the samples including density, open porosity, flexural strength, and flexural modulus are presented in Table 1. After densified with SiB_4 and SiC, flexural strength and modulus of the porous CVI C/SiC composites increased from 135 to 330 MPa and from 25 to 30 GPa, respectively. After coated with two layers of SiC coating, strength and modulus of the modified C/SiC composites only slightly increased to 340 MPa and 36 GPa, respectively, corresponding to the noticeable decrease in the porosity. As a comparison, when the porous CVI C/SiC composites with a density of 1.63 g/cm^3, sample A, was coated with two layers of SiC coating, the composites, sample B, attained a flexural strength of 222 MPa and a flexural modulus of 25 GPa.

Known from the flexural stress–strain curves of the samples (Fig. 6), the modified composites had improved flexural strength and modulus, which exhibited a non-catastrophic failure behavior. Porous C/SiC (sample A) had high porosity, and matrix could not transfer the stress effectively to the fibers. Therefore, when the stress reached the maximum, sample A consumed the minimum work of fracture, which can be estimated from the area beneath the stress–strain curves. As a comparison, the SiB_4 modified C/SiC composites (samples D and E) could consume much higher work of fracture. The improvement of the mechanical properties is owing to the densification of the matrix which plays a key role in stress transferring. During loading, stress can be effectively transferred from dense matrix to the PyC interphase and the carbon fibers. As a compliant interfacial layer, PyC interphase may release the thermal residual stresses between the dense matrix and the carbon fibers. Matrix micro-cracks propagating in the dense SiC–SiB_4 matrix can be deflected in the PyC interphase, leading to the pullout of the carbon fibers (Fig. 7). As a result, the dense C/SiC–SiB_4 composites showed improved mechanical properties.

3.3. Thermal shock resistance of composites

The thermal shock resistances of samples B and E were compared, which were air-quenched from 1300 °C to room tem-

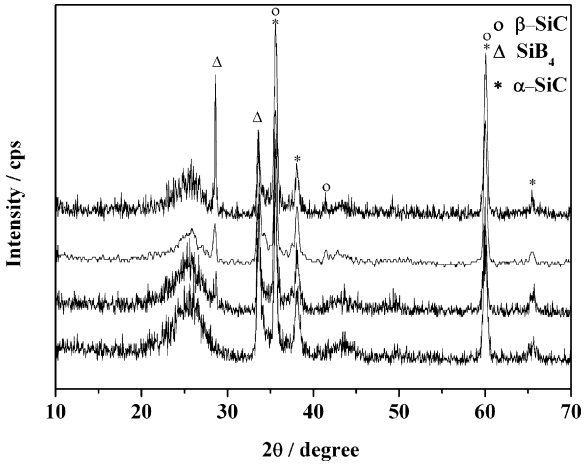

Fig. 5. Microarea XRD patterns of sample D.

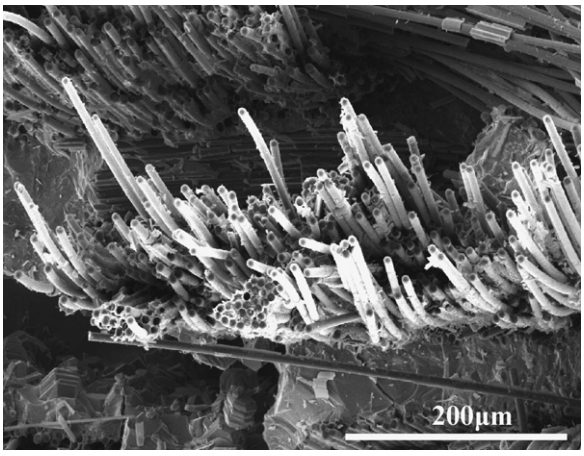

Fig. 7. SEM image on the fracture surface of sample D.

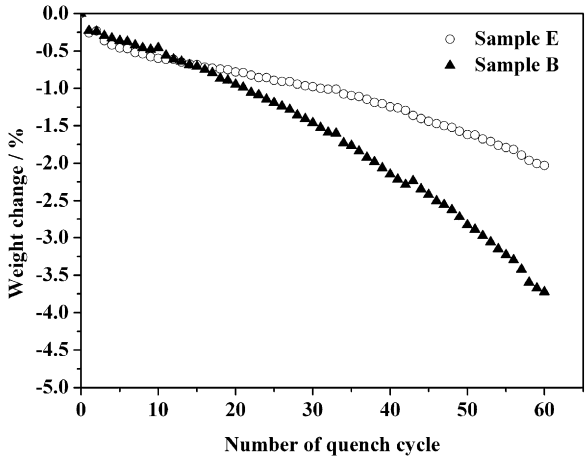

Fig. 8. Effect of thermal shock cycle number on the weight changes of samples B and E.

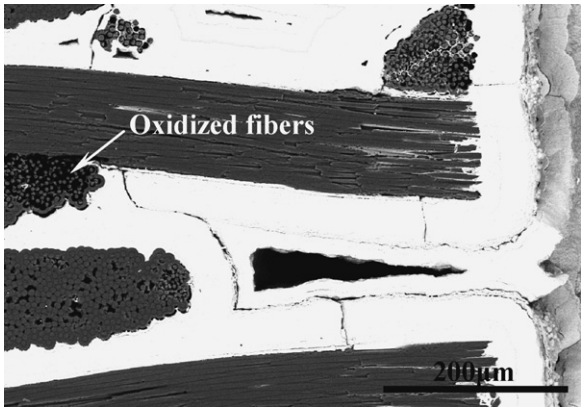

Fig. 9. Back-scattered electron image on the polished cross-section of sample B, showing carbon fibers were oxidized due to the inward diffusion of oxygen through micro-cracks.

perature for 60 cycles. Fig. 8 illustrates the effect of thermal shock cycle number on the weight losses of samples B and E, and the weight losses were both increased continuously due to the oxidation. When samples B and E were thermally shocked for less than 20 cycles, they had a similar weight loss due to the inwards diffusion of oxygen through the matrix/coating micro-cracks which led to the consumption of carbon phase. With increasing thermal shock cycles, weight loss of sample B continued to increase, because the large open porosity and matrix micro-cracks applied channels for the in-depth diffusion of oxygen, leading to the oxidation of carbon fibers (Fig. 9). For sample E, with the increase of thermal shock cycles, the reaction between SiB_4 and O_2 led to the formation of B_2O_3 and SiO_2 as glass sealant, which filled the matrix micro-cracks, as shown in Fig. 10(b). The glass sealant hindered the inwards diffusion of oxygen and protected carbon fibers against oxidation (Fig. 10(a)). The weight loss of the sample E kept slowly increasing due to the volatilization of B_2O_3 at high temperatures.[13,14]

A temperature difference was produced by the sudden change in the surrounding temperature, and thermal stress was generated in the composites. The matrix thermal stress (σ_m) created due to the temperature difference is expressed by:

$$\sigma_m = E_m(\alpha_c - \alpha_m)\Delta T \tag{6}$$

where ΔT is the temperature difference, α_c and α_m are the coefficient of thermal expansion of composite and matrix, respectively. E_m is the flexural modulus of matrix. α_c can be expressed as the following equation:

$$\alpha_c = \frac{\alpha_f E_f V_f + \alpha_m E_m(1 - V_f)}{E_f V_f + E_m(1 - V_f)} \tag{7}$$

where V_f is the fiber fraction of composites, E_f is the modulus of fiber and α_f is the coefficient of thermal expansion of fiber. Regarding Eqs. (6) and (7), an expression for matrix thermal stress can be expressed as Eq. (8):

$$\sigma_m = \Delta T \frac{\alpha_f - \alpha_m}{(V_f/E_m) + (1 - V_f)/E_f} V_f \tag{8}$$

According to Eq. (8), matrix thermal stress is related to the coefficient of thermal expansion of matrix and the matrix modulus. With the decreases of the coefficient of thermal expansion of matrix and the matrix modulus, the thermal stress in the matrix decrease, as well as in the fiber, leading to an increase in strength of the composites. The flexural strength and the

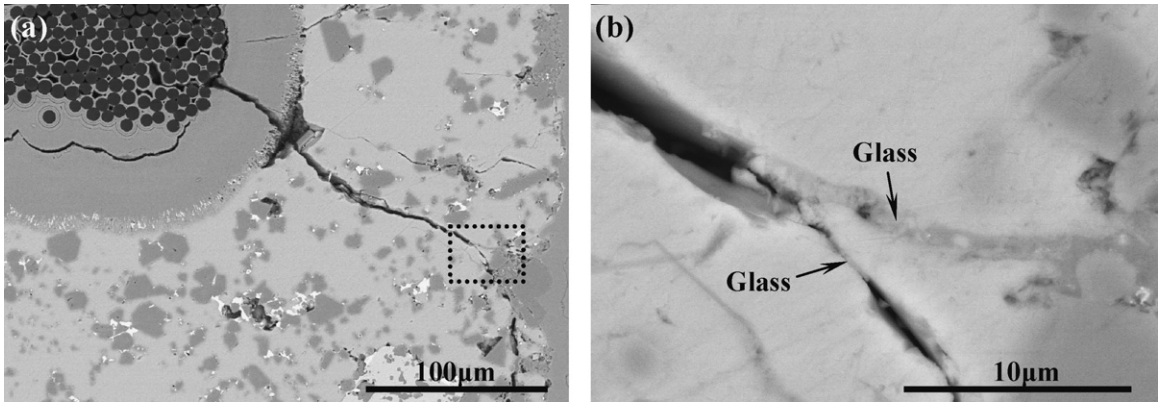

Fig. 10. Back-scattered electron images on the polished cross-section of the sample E after thermal shock test for 60 cycles: (a) low magnification image showing the fibers were protected against oxidation and (b) high magnification image showing the matrix micro-cracks was self-healed by the formation of glass.

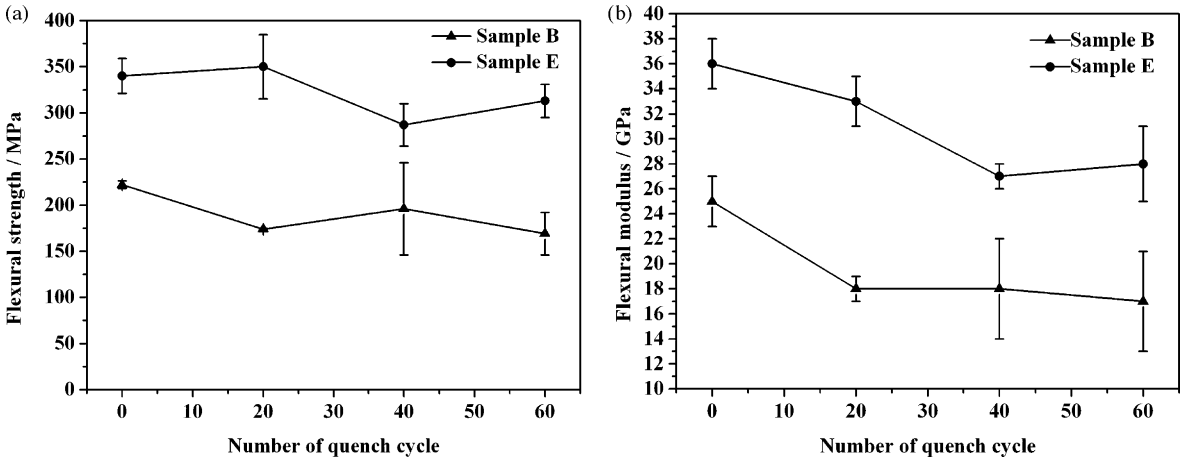

Fig. 11. Effect of thermal shock cycle number on the mechanical properties of samples B and E: (a) the flexural strength and (b) the flexural modulus.

flexural modulus of samples B and E as a function of quench cycle number are shown in Fig. 11(a) and (b). As shown in Fig. 11(b), with the increase of quench cycle number, the flexural modulus of samples decreased gradually. When sample E was thermally shocked for less than 20 cycles, the coefficient of thermal expansion of fiber and matrix gradually matched and the thermal stress decreased gradually, leading to the increase of the flexural strength. With the further increase of the quench cycle number, the flexural strength decreased due to the consumption of carbon phase. For sample E, when quenching cycle number continued to increase, micro-cracks in the SiC matrix were healed by borosilicate glass formed by the oxidation of SiB_4. As a result, the residual flexural strength of sample E retained 95% of the original strength after thermal shock test for 60 cycles. As a comparison, there were more pores in sample B and the matrix/coating micro-cracks cannot be effectively healed at 1300 °C, leading to the continuous consumption of carbon phase. As a result, the flexural strength of sample B decreased by 24% after 60 cycles of thermal shock.

4. Conclusions

The current work reported on the synthesis mechanism of SiB_4 from the B_4C–Si system. Silicon atoms begin to diffuse into the interstitial site of B_4C crystal lattice at 1300 °C with the formation of solid solution of $B_{12}(C, Si, B)_3$. Above 1400 °C, SiB_4 can be formed due to the replacement of C atoms in B_4C by silicon atoms. The amount of in situ formed SiB_4 increased with the increase of reaction temperature. According to the reactive synthesis mechanism of SiB_4, B_4C particles were infiltrated into the inter-bundle pores of porous 2D C/SiC composites by slurry infiltration, which reacted with molten silicon at 1500 °C, leading to the in situ formation of C/SiC–SiB_4 composites. Compared with CVI C/SiC composites, the mechanical properties and thermal shock resistance of C/SiC–SiB_4 composite were greatly improved.

Acknowledgements

Authors wish to thank the National Nature Science Foundation of China (project no. 50972119), the program for New Century Excellent Talents in University and Sci-tech Innovation Foundation of Northwestern Polytechnical University (project no. W016147) for their financial supports.

References

1. Naslain R. Design, preparation and properties of non-oxide CMCs for application in engines and nuclear reactors: an overview. *Compos Sci Technol* 2004;**64**:155–70.
2. Nakano K, Kamiya A, Ogawa H, Nishino Y. Fabrication and mechanical properties of carbon fiber reinforced silicon carbide composites. *J Jpn Ceram Soc* 1992;**100**:472–5.
3. Besmann TM, Sheldon BW, Lowden RA, Stinton DP. Vapor-phase fabrication and properties of continuous-filament ceramic composites. *Science* 1991;**253**:1104–9.
4. Krenkel W, Berndt F. C/C–SiC composites for space applications and advanced friction systems. *Mater Sci Eng A* 2005;**412**:177–81.
5. Staehler James M, Mall Shankar, Zawada Larry P. Frequency dependence of high-cycle fatigue behavior of CVI C/SiC at room temperature. *Compos Sci Technol* 2003;**63**:2121–31.
6. Lamouroux F, Bourrat X, Naslain R. Structure/oxidation behavior relationship in the carbonaceous of 2D-C/PyC/SiC composites. *Carbon* 1993;**31**:1273–88.
7. Xu YD, Cheng LF, Yan DT, Zhang LT. Microstructure and mechanical properties of three-dimensional carbon/silicon carbide composites fabricated by chemical vapor infiltration. *Carbon* 1998;**36**:1051–6.
8. Xu YD, Cheng LF, Zhang LT. Carbon/silicon carbide composites prepared by chemical vapor infiltration combined with silicon melt infiltration. *Carbon* 1999;**37**:1179–87.
9. Mall Shankar, John Mark Engesser. Effects of frequency on fatigue behavior of CVI C/SiC at elevated temperature. *Compos Sci Technol* 2006;**66**:863–74.
10. Yin XW, Cheng LF, Zhang LT, Xu YD, Luan XG. Oxidation behavior of three-dimensional woven C/SiC composites. *Mater Sci Technol* 2001;**17**:727–30.
11. Naslain R, Guette A, Rebillat F, Pailler R, Langlais F, Bourrat X. Boron-bearing species in ceramic matrix composites for long-term aerospace applications. *J Solid State Chem* 2004;**177**:449–56.
12. Samsonov GV, Sleptsov VM. Preparation of boron–silicon alloys. *Powder Metall Met Ceram* 1964;**3**:488–96.
13. Matsushita JI, Sawada Y. Oxidation resistance of silicon tetra boride powder. *J Jpn Ceram Soc* 1997;**105**:922–4.
14. Tong CQ, Cheng LF, Yin XW, Zhang LT, Xu YD. Oxidation behavior of 2D C/SiC composite modified by SiB_4 particles in inter-bundle pores. *Compos Sci Technol* 2008;**68**:602–7.
15. Corman GS, Dean AJ, Brabetz S, Brun MK, Luthra KL, Tognarelli L, et al. Rig and engine testing of melt infiltrated ceramic composites for combustor

and shroud applications. *J Eng Gas Turbines Powder: Trans Am Soc Mech Eng* 2002;**124**:459–64.
16. Brennan JJ. Interfacial characterization of a slurry–cast melt–infiltrated SiC/SiC ceramic–matrix composite. *Acta Mater* 2000;**48**:4619–28.
17. Gern FH, Kochendörfer R. Liquid silicon infiltration: description of infiltration dynamics and silicon carbide formation. *Compos Part A* 1997;**28**:355–64.
18. Heidenreich Bernhard. In: Krenkel Walter, editor. *Ceramic Matrix Composites: Fiber Reinforced Materials and their Applications*. E-Publishing Inc.; 2008. p. 119–21.
19. Singh M, Behrendt DR. Microstructure and mechanical properties of reaction-formed silicon carbide (RFSC) ceramics. *Mater Sci Eng A* 1994;**187**:183–7.
20. Singh M, Behrendt DR. Reactive melt infiltration of silicon–molybdenum alloys into microporous carbon preforms. *Mater Sci Eng A* 1995;**194**:193–200.
21. Panasyuk AD, Oreshkin VD, Maslennikova VR. Kinetics of the reactions of boron carbide with liquid aluminum, silicon, nickel and iron. *Powder Metall Met Ceram* 1979;**18**:487–90.
22. Xu YD, Cheng LF, Zhang LT, Yin HF, Yin XW, You C. Effects of chemical vapor infiltration atmosphere on the mechanical properties and microstructure of carbon fibers. *J Eur Ceram Soc* 2001;**21**: 809–16.
23. Lazzari R, Vast N, Besson JM, Baroni S, Dal Corso A. Atomic structure and vibrational properties of icosahedral B_4C boron carbide. *Phys Rev Lett* 1999;**83**:3230–3.
24. Messner Robert P, Chiang Yet-Ming. Liquid-phase reaction-bonding of silicon carbide using alloyed silicon–molybdenum melts. *J Am Ceram Soc* 1990;**73**:1193–200.
25. Scherer GW. Correction of "drying gels. I. General theory". *J NonCryst Solids* 1987;**92**:375–82.